International Journal of Plasticity 32–33 (2012) 59–69

Contents lists available at SciVerse ScienceDirect

International Journal of Plasticity

journal homepage: www.elsevier.com/locate/ijplas

An elasto-viscoplastic formulation based on fast Fourier transforms for the prediction of micromechanical fields in polycrystalline materials

Ricardo A. Lebensohn [a,*], Anand K. Kanjarla [a], Philip Eisenlohr [b]

[a] Materials Science and Technology Division, Los Alamos National Laboratory, MS G755, Los Alamos, NM 87845, USA
[b] Max-Planck-Institut für Eisenforschung, Max-Planck-Str. 1, 40237 Düsseldorf, Germany

ARTICLE INFO

Article history:
Received 26 August 2011
Received in final revised form 12 December 2011
Available online 28 December 2011

Keywords:
B. Polycrystalline material
B. Anisotropic material
B. Elastic-viscoplastic material
B. Crystal plasticity
A. Microstructures

ABSTRACT

We present the infinitesimal-strain version of a formulation based on fast Fourier transforms (FFT) for the prediction of micromechanical fields in polycrystals deforming in the elasto-viscoplastic (EVP) regime. This EVP extension of the model originally proposed by Moulinec and Suquet to compute the local and effective mechanical behavior of a heterogeneous material directly from an image of its microstructure is based on an implicit time discretization and an augmented Lagrangian iterative procedure. The proposed model is first benchmarked, assessing the corresponding elastic and viscoplastic limits, the correct treatment of hardening, rate-sensitivity and boundary conditions, and the rate of convergence of the numerical method. In terms of applications, the EVP–FFT model is next used to examine how single crystal elastic and plastic directional properties determine the distribution of local fields at different stages of deformation.

© 2011 Elsevier Ltd. All rights reserved.

1. Introduction

Polycrystalline materials play a fundamental role as structural and functional materials in current and future technological applications. The mechanical properties of plastically deforming polycrystals are dictated, on the one hand, by the structure and dynamics of crystalline defects, like vacancies and interstitials, dislocations, grain boundaries, voids, and, on the other hand, by the size, morphology, spatial distribution and orientation of the constituent single crystal grains, i.e. in a broad sense, by the texture of the polycrystal. From an experimental point of view, powerful techniques are emerging to fully characterize polycrystal textures in three dimensions (3-D) and follow its in situ evolution during thermo-mechanical processing. For example, serial-sectioning by Focus-Ion-Beam (FIB) combined with Electron Back-Scattering Diffraction (EBSD) is by now a well established tool to characterize (destructively) local orientations in 3-D (e.g. Uchic et al., 2006) with nanometric spatial resolution. Also, synchrotron-based X-ray diffraction can now be used for in situ measurement of the positions, shapes, and crystallographic orientations (e.g. Lauridsen et al., 2006) and local elastic strains of bulk grains in an aggregate (Oddershede et al., 2010, 2011), with micrometric and sub-micrometric resolution, in a non-destructive fashion.

From a modeling perspective, the challenge arising from these novel experimental techniques, which produce very large 3-D digital images of the microstructure (i.e. crystal orientation and/or the phase identification given on a regular grid of points with intragranular resolution) is to devise new, robust and very efficient numerical formulations for interpretation and exploitation of the massive amount of data generated by these measurements.

As a contribution to face this challenge, we present here an extension to the most general elasto-viscoplastic (EVP) deformation regime of a modeling technique originally developed by Suquet and co-workers (Moulinec and Suquet, 1994, 1998;

* Corresponding author. Tel.: +1 505 665 3035; fax: +1 505 667 8021.
E-mail addresses: lebenso@lanl.gov (R.A. Lebensohn), anand@lanl.gov (A.K. Kanjarla), p.eisenlohr@mpie.de (P. Eisenlohr).

0749-6419/$ - see front matter © 2011 Elsevier Ltd. All rights reserved.
doi:10.1016/j.ijplas.2011.12.005

Michel et al., 2000, 2001) as an efficient method to compute the micromechanical fields of periodic heterogeneous materials directly from an image of their microstructure. Under this technique, which in the past we have extended, implemented and applied to polycrystals deforming in the more restricted elastic (Brenner et al., 2009) and the rigid-viscoplastic (Lebensohn, 2001; Lebensohn et al., 2008, 2009; Lee et al., 2011) regimes, the input microstructural image is treated using the Fast Fourier Transform (FFT) algorithm to solve the corresponding micromechanical problem. The present extension of the FFT-based model to the EVP regime is a necessary step towards expanding its applicability to open problems involving polycrystal plasticity, like the prediction of internal stresses with intragranular resolution for interpretation of either space-resolved or global measurements, or the modeling of the role played by texture and microstructure on the distribution of extreme values of the micromechanical fields, which in turn determine the macroscopic mechanical behavior of polycrystalline aggregates during cyclic deformation, to mention some of the most challenging and relevant problems.

While the finite element method (FEM) has been extensively used to deal with problems involving crystal plasticity (CP) in the elastoplastic regime (e.g. Mika and Dawson, 1998; Barbe et al., 2001a, 2001b; Raabe et al., 2001; Bhattacharyya et al., 2001; Diard et al., 2005; Delannay et al., 2006; and the comprehensive review of Roters et al., 2010), the large number of degrees of freedom required by FEM calculations with direct input from microstructural images constitutes an objective limitation for the size of the polycrystalline aggregates that can be treated with CP-FEM, within reasonable computing times. Conceived as an efficient alternative to FEM, the FFT-based methodology can account for fine-scale microstructural information with a level of fidelity, in practice, unreachable with FEM. One disadvantage of FFT-based formulations is the requirement of periodic microstructures, making them less general than FEM.

The plan of the paper is as follows. In Section 2 we present the extension of the FFT-based formulation to the case of polycrystals deforming in the elasto-viscoplastic regime. In Section 3 we benchmark the EVP–FFT formulation, including: (a) the assessment of the corresponding elastic (EL) and viscoplastic (VP) limits by comparison with earlier elastic (EL-FFT) and viscoplastic (VP-FFT) implementations, (b) the correct treatment of hardening, rate-sensitivity and boundary conditions, and (c) a detailed convergence analysis. In Section 4 we show an application of the EVP–FFT model to study how the single crystal elastic and plastic directional properties determine the distribution of local stresses in the initial elastic loading, the elastoplastic transition and the fully plastic regime, and, consequently, how this crystal anisotropy impacts the aforementioned transition at macroscopic level. In Section 5 we summarize and provide some perspectives for future applications of the EVP–FFT formulation.

2. Model

The FFT-based formulation is conceived for periodic unit cells and provides an exact solution (within the limitations imposed by the required discretization and the iterative character of the numerical algorithm) of the governing equations of equilibrium and compatibility, in such a way that the final (converged) equilibrated stress and compatible strain fields fulfill the required constitutive relation, at every discrete material point. The method was originally developed for linear (elastic) (Moulinec and Suquet, 1994, 1998), and nonlinear elastoplastic (Moulinec and Suquet, 1994, 1998) and viscoplastic (Michel et al., 2000, 2001) composites, with the goal of computing local and effective mechanical responses directly from pixel-based optical images of these materials, in which the source of heterogeneity is related to the spatial distribution of phases with different mechanical properties and image contrasts. Later, the FFT-based formulation was extended to linear and nonlinear polycrystals. In this case, the heterogeneity is related to the spatial distribution of crystals with directional mechanical properties, which can be identified by means of orientation images.

Briefly, the FFT-based formulation consists in iteratively adjusting a compatible strain (or strain-rate) field, related with an equilibrated stress field through a constitutive potential, such that the average of local work (or power) is minimized. Owing to the periodicity of the unit cell, periodic Green functions, convolution integrals and Fourier transforms can be efficiently utilized to solve the micromechanical problem (details are given in next section).

Regarding the specific iterative procedure required to solve a given micromechanical problem, several versions of the FFT-based method are presently available. The original formulation of Moulinec and Suquet (1994, 1998), known as the "basic" scheme, has been proven to converge for linear materials at a rate proportional to the local contrast in mechanical properties. To improve the convergence of this basic scheme, accelerated schemes have been proposed by different authors (Eyre and Milton, 1999; Brisard and Dormieux, 2010; Zeman et al., 2010). When the mechanical contrast is infinite and therefore convergence of the basic algorithm is not ensured, Michel et al. (2000, 2001) proposed an "augmented Lagrangians" scheme, which consists in adjusting two strain (or strain-rate) and two stress fields. By construction, one of the strain fields is compatible, and one of the stress fields fulfills equilibrium. Meanwhile, the constitutive equation relates the other strain and stress fields. The iterative procedure is designed to make the pairs of strain and stress fields converge to each other. At convergence, the method delivers a compatible strain field related to an equilibrated stress field through the local constitutive equation.

2.1. Elasto-viscoplastic formulation

As mentioned above, for plastically deforming polycystals, a version of the FFT-based model based on the popular rigid-viscoplastic approximation to crystal plasticity (Asaro and Needleman, 1985) is available (Lebensohn, 2001; Lebensohn et al.,

2008, 2009; Lee et al., 2011). Under this approximation, the elastic strains are considered negligible compared with the plastic strains and the viscoplastic strain rate $\dot{\boldsymbol{\varepsilon}}^p(\mathbf{x})$ is constitutively related with the stress $\boldsymbol{\sigma}(\mathbf{x})$ at a single-crystal material point $\mathbf{x}$ through a sum over the N active slip systems, of the form:

$$\dot{\boldsymbol{\varepsilon}}^p(\mathbf{x}) = \sum_{s=1}^{N} \mathbf{m}^s(\mathbf{x})\dot{\gamma}^s(\mathbf{x}) = \dot{\gamma}_o \sum_{s=1}^{N} \mathbf{m}^s(\mathbf{x}) \left(\frac{|\mathbf{m}^s(\mathbf{x}) : \boldsymbol{\sigma}(\mathbf{x})|}{\tau_o^s(\mathbf{x})} \right)^n \operatorname{sgn}(\mathbf{m}^s(\mathbf{x}) : \boldsymbol{\sigma}(\mathbf{x})) \tag{1}$$

where $\dot{\gamma}^s(\mathbf{x})$, $\tau_o^s(\mathbf{x})$ and $\mathbf{m}^s(\mathbf{x})$ are, respectively, the shear rate, the critical resolved shear stress (CRSS) and the Schmid tensor, associated with slip system (s) at point $\mathbf{x}$; $\dot{\gamma}_o$ is a normalization factor and n is the stress exponent (inverse of the rate-sensitivity exponent). Note that, in general, $\tau_o^s(\mathbf{x}, \boldsymbol{\varepsilon}^p(\boldsymbol{\sigma}(\mathbf{x})))$, i.e. the CRSS of slip system (s) is a function of accumulated plastic strain in the crystal (in turn a function of the stress) due to the strain-hardening of the slip systems. The resulting VP-FFT formulation, in combination with the augmented Lagrangians scheme, and (when necessary for large deformation predictions) with an Eulerian description of motion, has proven to be very useful for predicting local fields with intragranular resolution, effective behavior, and microstructure evolution of polycrystals deforming in a fully-plastic regime. However, while neglecting elastic effects simplifies the formulation and speeds up considerably its numerical performance, the VP-FFT formulation cannot be used in problems in which the elastic and plastic strains are comparable in magnitude and/or when the full stress tensor field (not just the deviatoric part of it) needs to be determined. The ability of a model to simultaneously account for elastic and viscoplastic effects in single crystals is obviously relevant to study phenomena like the build-up of internal elastic strains responsible for measurable changes in lattice spacing, or the development of stress concentrations leading to damage during cyclic deformation/incipient plasticity, etc.

The solution of an EVP problem involves the adoption of an appropriate time discretization scheme. Using an Euler implicit time discretization and Hooke's law, the expression, in small strains, of the stress in material point $\mathbf{x}$ at $t + \Delta t$ is given by

$$\boldsymbol{\sigma}^{t+\Delta t}(\mathbf{x}) = \mathbf{C}(\mathbf{x}) : \boldsymbol{\varepsilon}^{e,t+\Delta t}(\mathbf{x}) = \mathbf{C}(\mathbf{x}) : \left(\boldsymbol{\varepsilon}^{t+\Delta t}(\mathbf{x}) - \boldsymbol{\varepsilon}^{p,t}(\mathbf{x}) - \dot{\boldsymbol{\varepsilon}}^{p,t+\Delta t}(\mathbf{x}, \boldsymbol{\sigma}^{t+\Delta t})\Delta t \right) \tag{2}$$

where $\boldsymbol{\sigma}(\mathbf{x})$ is the Cauchy stress tensor, $\mathbf{C}(\mathbf{x})$ is the elastic stiffness tensor, $\boldsymbol{\varepsilon}(\mathbf{x})$, $\boldsymbol{\varepsilon}^e(\mathbf{x})$, and $\boldsymbol{\varepsilon}^p(\mathbf{x})$ are the total, elastic and plastic strain tensors, and $\dot{\boldsymbol{\varepsilon}}^p(\mathbf{x})$ is the plastic strain-rate tensor given, e.g. by Eq. (1). In what follows, the supra-indices $t + \Delta t$ will be omitted, i.e. the time-dependent stress and strain fields with no time supra-index correspond to time $(t + \Delta t)$, and only fields corresponding to the previous time step (t) will be explicitly indicated. Constitutive Eq. (2) and its inverse relation then read:

$$\boldsymbol{\sigma}(\mathbf{x}) = \mathbf{C}(\mathbf{x}) : \left(\boldsymbol{\varepsilon}(\mathbf{x}) - \boldsymbol{\varepsilon}^{p,t}(\mathbf{x}) - \dot{\boldsymbol{\varepsilon}}^{p}(\mathbf{x}, \boldsymbol{\sigma})\Delta t \right) \tag{3}$$

$$\boldsymbol{\varepsilon}(\mathbf{x}) = \mathbf{C}^{-1}(\mathbf{x}) : \boldsymbol{\sigma}(\mathbf{x}) + \boldsymbol{\varepsilon}^{p,t}(\mathbf{x}) + \dot{\boldsymbol{\varepsilon}}^{p}(\mathbf{x}, \boldsymbol{\sigma})\Delta t \tag{4}$$

2.2. Green function method

Adding and subtracting from the stress tensor an appropriate expression involving $\mathbf{C}^o$, the stiffness of a reference linear medium, gives (using explicit index notation):

$$\sigma_{ij}(\mathbf{x}) = \sigma_{ij}(\mathbf{x}) + C^o_{ijkl}u_{k,l}(\mathbf{x}) - C^o_{ijkl}u_{k,l}(\mathbf{x}) \tag{5}$$

where $u_{k,l}(\mathbf{x})$ is the displacement-gradient tensor, i.e. $\varepsilon_{kl}(\mathbf{x}) = (u_{k,l}(\mathbf{x}) + u_{k,l}(\mathbf{x}))/2$.

Conveniently regrouping terms in Eq. (5):

$$\sigma_{ij}(\mathbf{x}) = C^o_{ijkl}u_{k,l}(\mathbf{x}) + \varphi_{ij}(\mathbf{x}) \tag{6}$$

where the polarization field is given by

$$\varphi_{ij}(\mathbf{x}) = \sigma_{ij}(\mathbf{x}) - C^o_{ijkl}u_{k,l}(\mathbf{x}) = \sigma_{ij}(\mathbf{x}) - C^o_{ijkl}\varepsilon_{kl}(\mathbf{x}) \tag{7}$$

Combining expression (7) with the equilibrium equation $\sigma_{ij,j}(\mathbf{x}) = 0$:

$$C^o_{ijkl}u_{k,lj}(\mathbf{x}) + \varphi_{ij,j}(\mathbf{x}) = 0 \tag{8}$$

Solving differential Eq. (8) for a periodic unit cell under an applied strain $\mathbf{E} = \langle \boldsymbol{\varepsilon}(\mathbf{x}) \rangle$ using Green function method requires writing the following auxiliary problem:

$$C^o_{ijkl}G_{km,lj}(\mathbf{x} - \mathbf{x}') + \delta_{im}\delta(\mathbf{x} - \mathbf{x}') = 0 \tag{9}$$

where $G_{km}(\mathbf{x})$ is the Green function associated with the displacement field $u_k(\mathbf{x})$. The solution for the displacement gradient is given by the convolution integral:

$$u_{k,l}(\mathbf{x}) = \int_{R^3} G_{ki,jl}(\mathbf{x} - \mathbf{x}')\varphi_{ij}(\mathbf{x}')d\mathbf{x}' \tag{10}$$

Solving Eq. (10) in Fourier space using the convolution theorem, the compatible strain field deriving from the solution of Eq. (8) is given by

$$\varepsilon_{ij}(\mathbf{x}) = E_{ij} + \mathrm{FT}^{-1}\left(\mathrm{sym}\left(\hat{\Gamma}^{o}_{ijkl}(\mathbf{k})\right)\hat{\varphi}_{kl}(\mathbf{k})\right) \tag{11}$$

where the symbol "^" indicates Fourier transform (FT) and $\mathbf{k}$ is a point (frequency) of Fourier space. The Green operator in Fourier space, which is only a function of the reference stiffness tensor and the frequency, is given by

$$\hat{\Gamma}^{o}_{ijkl}(\mathbf{k}) = -k_j k_l \hat{G}_{ik}(\mathbf{k}) \tag{12}$$

With

$$\hat{G}_{ik}(\mathbf{k}) = [C^{o}_{kjil} k_l k_j]^{-1}$$

Note that, while Eqs. (1)–(12) are valid for arbitrary material points $\mathbf{x}$ and frequencies $\mathbf{k}$, the numerical method consists in evaluating these expressions in points and frequencies belonging to regular grids (of the same size) in Cartesian and Fourier spaces, respectively, in which case, the direct and inverse Fourier Transforms in Eq. (11) become discrete, and the FFT algorithm can be applied.

2.3. Iterative procedure

Since the polarization field, defined in Eq. (7), is precisely a function of the strain field $\boldsymbol{\varepsilon}(\mathbf{x})$, i.e. the sought solution of differential Eq. (8), some kind of iterative procedure is required to solve the problem. Let assume that $\lambda^{(i)}_{ij}$ and $e^{(i)}_{ij}$ are, respectively, auxiliary guess stress and strain fields at iteration (i). The polarization field then reads:

$$\varphi^{(i)}_{ij}(\mathbf{x}) = \lambda^{(i)}_{ij}(\mathbf{x}) - C^{o}_{ijkl} e^{(i)}_{kl}(\mathbf{x}) \tag{13}$$

and the new guess for the strain field is given by (c.f. Eq. (11)):

$$e^{(i+1)}_{ij}(\mathbf{x}) = E_{ij} + \mathrm{FT}^{-1}\left(\mathrm{sym}\left(\hat{\Gamma}^{o}_{ijkl}(\mathbf{k})\right)\hat{\phi}^{(i)}_{kl}(\mathbf{k})\right) \tag{14}$$

An alternative fix-point expression, which requires computing the Fourier transform of the stress field instead of that of the polarization field is given by (Michel et al., 2001):

$$e^{(i+1)}_{ij}(\mathbf{x}) = E_{ij} + \mathrm{FT}^{-1}\left(\hat{\hat{e}}^{(i)}_{ij} + \mathrm{sym}\left(\hat{\Gamma}^{o}_{ijkl}(\mathbf{k})\right)\hat{\lambda}^{(i)}_{kl}(\mathbf{k})\right) \tag{15}$$

With $e^{(i+1)}_{ij}(\mathbf{x})$ obtained from Eq. (15), one possibility, following the "basic" scheme of Moulinec and Suquet (1994, 1998), is to replace its value in Eq. (3) and solve a set of 6 nonlinear equations to obtain the six unknown independent components of $\lambda^{(i+1)}_{ij}(\mathbf{x})$. However, in our implementation, we chose to use the more involved, but also more robust and faster to converge augmented Lagrangians scheme, adapted from Michel et al. (2000, 2001). This scheme requires, for every material point $\mathbf{x}$, the nullification of a residual $\mathbf{R}$, which is a function of the stress tensor $\boldsymbol{\sigma}^{(i+1)}$ constitutively related with the strain tensor $\boldsymbol{\varepsilon}^{(i+1)}$ (in what follows, the dependence with $\mathbf{x}$ will be omitted):

$$R_k\left(\boldsymbol{\sigma}^{(i+1)}\right) = \sigma^{(i+1)}_k + C^{o}_{kl}\varepsilon^{(i+1)}_l\left(\boldsymbol{\sigma}^{(i+1)}\right) - \lambda^{(i)}_k - C^{o}_{kl} e^{(i+1)}_l = 0 \tag{16}$$

Note that for convenience in Eq. (16) the residual is written in contracted notation for symmetric tensors, e.g. $\sigma_{ij} \to \sigma_k, k = 1,6; C_{ijmn} \to C_{kl}, k,l = 1,6$, etc. Nonlinear Eq. (16) is solved using a scheme of the Newton–Raphson (N–R) type, i.e.

$$\sigma^{(i+1,j+1)}_k = \sigma^{(i+1,j)}_k - \left(\left.\frac{\partial R_k}{\partial \sigma_l}\right|_{\boldsymbol{\sigma}^{(i+1,j)}}\right)^{-1} R_l\left(\boldsymbol{\sigma}^{(i+1,j)}\right) \tag{17}$$

is the expression that gives the $(j+1)$-guess for the stress field $\sigma^{(i+1)}_k$. Using Eq. (16) and the constitutive relation (Eq. (4)), the Jacobian in the above expression reads:

$$\left.\frac{\partial R_k}{\partial \sigma_l}\right|_{\boldsymbol{\sigma}^{(i+1,j)}} = \delta_{kl} + C^{o}_{kq} C^{-1}_{ql} + \Delta t\; C^{o}_{kq}\left.\frac{\partial \dot{\varepsilon}^{p}_q}{\partial \sigma_l}\right|_{\boldsymbol{\sigma}^{(i+1,j)}} \tag{18}$$

The derivative on the right is the tangent compliance of the viscoplastic relation (Eq. (1)). Noting that, due to the dependence of the plastic strain on the stress, the CRSS is a function of the stress $\tau^{s}_{o}(\varepsilon^{p}(\boldsymbol{\sigma})) = \tau^{s}_{o}(\boldsymbol{\sigma})$, an approximate expression for this tangent compliance is given by

$$\left.\frac{\partial \dot{\varepsilon}^{p}_q}{\partial \sigma_l}\right|_{\sigma^{(i+1,j)}} \cong n\dot{\gamma}_o \sum_{s=1}^{N} \frac{m^{s}_q m^{s}_l}{\tau^{s}_{o}\left(\boldsymbol{\sigma}^{(i+1,j)}\right)}\left(\frac{\mathbf{m}^{s} : \boldsymbol{\sigma}}{\tau^{s}_{o}\left(\boldsymbol{\sigma}^{(i+1,j)}\right)}\right)^{n-1} \tag{19}$$

In writing Eq. (19), we have neglected the term $\partial\tau^{s}_{o}/\partial\sigma_j$, which, besides complicating the above expression, depends on the specific functional form of the adopted hardening law. Consequently, combining Eqs. (18) and (19):

$$\left.\frac{\partial R_k}{\partial \boldsymbol{\sigma}_1}\right|_{\boldsymbol{\sigma}^{i+1,j}} \cong \delta_k l + C^o_{kq} C^{-1}_{ql} + (\Delta t\ n\dot{\gamma}_o) C^o_{kq} \sum_{s=1}^{N} \frac{m^s_q m^s_l}{\tau^s_o(\boldsymbol{\sigma}^{(i+1,j)})} \left(\frac{\mathbf{m}^s : \boldsymbol{\sigma}}{\tau^s_o(\boldsymbol{\sigma}^{(i+1,j)})}\right)^{n-1} \tag{20}$$

gives an approximate Jacobian (strictly, not Newton–Raphson's tangent operator). In spite of this approximation, the convergence rate is almost unaffected, even in the case of strong strain-hardening, compared with the no hardening case (see Section 3).

Once convergence is achieved on $\boldsymbol{\sigma}^{(i+1)}$ (and thus on $\boldsymbol{\varepsilon}^{(i+1)}$), the new guess for the auxiliary stress field $\boldsymbol{\lambda}$ is given by

$$\boldsymbol{\lambda}^{(i+1)}(\mathbf{x}) = \boldsymbol{\lambda}^{(i)}(\mathbf{x}) + \mathbf{C}^o : \left(\mathbf{e}^{(i+1)}(\mathbf{x}) - \boldsymbol{\varepsilon}^{(i+1)}(\mathbf{x})\right) \tag{21}$$

and the algorithm advances (c.f. Eq. (15)), until the normalized average differences between the stress fields $\boldsymbol{\sigma}(\mathbf{x})$ and $\boldsymbol{\lambda}(\mathbf{x})$, and the strain fields $\boldsymbol{\varepsilon}(\mathbf{x})$ and $\mathbf{e}(\mathbf{x})$, are smaller than a threshold. In all the examples that follow, we used a threshold of 10^{-5}. This condition also implies fulfillment of equilibrium and compatibility (Michel et al., 2001) up to such precision.

2.4. Boundary conditions

While the algorithm described above solves the problem for a strain imposed to the unit cell of the form:

$$E_{ij} = E^t_{ij} + \dot{E}_{ij}\Delta t \tag{22}$$

the actual boundary conditions applied to the unit cell can be mixed, i.e. some components of macroscopic strain rate $\dot{E}_{ij}$ and some complementary components of the macroscopic stress Σ_{ij} may be imposed (e.g. in the case of tension along x_3 with no shear strains allowed, $\dot{E}_{33} > 0$ and $\dot{E}_{23} = \dot{E}_{31} = \dot{E}_{12} = 0$ and $\Sigma_{11} = \Sigma_{22} = 0$ are the imposed strain-rate and stress components), or even the full stress tensor may be prescribed (i.e. creep). In such cases, the algorithm should include the following extra step, after $\boldsymbol{\lambda}^{(i+1)}(\mathbf{x})$ is determined (Eq. (21)). If component Σ_{pq} is imposed, the corresponding $(i+1)$-guess for strain component $E^{(i+1)}_{pq}$ is obtained as (Michel et al., 2001):

$$E^{(i+1)}_{pq} = E^{(i)}_{pq} + C^{o-1}_{pqkl}\alpha^{[kl]}\left(\Sigma_{kl} - \left\langle \lambda^{(i+1)}_{kl}(\mathbf{x})\right\rangle\right) \tag{23}$$

where $\alpha^{[kl]} = 1$ if component Σ_{kl} is imposed, and zero otherwise.

2.5. Hardening law

While, as discussed above, the approximate expression for the Jacobian (Eq. (19)) allows us to use different hardening laws without changing the proposed EVP algorithm, in what follows we present cases with either no strain-hardening (i.e. τ^s_o constant), or a very simple linear hardening, i.e.

$$\Delta\tau^s_o = H\Delta\Gamma \tag{24}$$

where H is a positive scalar and $\Delta\Gamma = \sum_{s=1}^{N}|\dot{\gamma}^s\Delta t|$.

3. Benchmarks

The first benchmark for the proposed EVP–FFT numerical scheme is to verify that the elastic and viscoplastic limits match the previous simpler EL-FFT and VP-FFT implementations. For this we have chosen the case of a copper polycrystal, represented by a periodic unit cell generated by Voronoi tessellation, consisting of 100 grains with randomly chosen orientations. The unit cell was discretized using a $128 \times 128 \times 128$ grid (same unit cell, discretized in the same fashion will be adopted throughout the examples presented in this paper). The adopted single crystal elastic constants correspond to copper at room temperature: $C_{11} = 170.2$ GPa, $C_{12} = 114.9$ GPa and $C_{44} = 61.0$ GPa (Simmons and Wang, 1971). The copper crystals deform plastically by slip on 12 $\{111\}\langle 110\rangle$ slip systems with a constant (i.e. no strain-hardening) CRSS value of $\tau^s_o = 10$ MPa $(s = 1,\ldots,12)$ and a stress exponent $n = 10$. The boundary conditions correspond to uniaxial tension along x_3, with an applied strain rate component along the tensile axis $\dot{E}_{33} = 1s^{-1}$. The EVP–FFT simulation was carried out in 30 steps of 0.01%, up to a strain of 0.3%. Fig. 1 shows: (a) the equivalent stress–strain curve predicted with the EVP–FFT model, together with two straight lines representing the effective responses predicted for the same unit cell by the EL-FFT (which gives the initial elastic slope) with the same elastic constants, and the by VP-FFT (which gives the saturated stress) adopting the same slip systems, CRSS and stress exponent respectively, and (b) the equivalent stress fields predicted by the EL-FFT and EVP–FFT models at 0.01%, and by the VP-FFT and EVP–FFT at 0.3%, respectively. The agreement of both the effective behavior and the von Mises local fields, between the EVP–FFT predictions and the corresponding EL and VP limits is excellent. We have also verified the good match between individual stress component fields, i.e. of the full stress tensor, in the elastic case; and of the deviatoric stress tensor, in the fully plastic case.

The second benchmark concerns the adequate treatment of strain-hardening and rate-sensitivity. Fig. 2 shows the stress–strain curves predicted for the copper polycrystal with the same elastic constants, slip systems, CRSS and stress exponent, and a linear strain-hardening, adopting H = 100 MPa (see Eq. (24)). Uniaxial stress boundary conditions are also the same

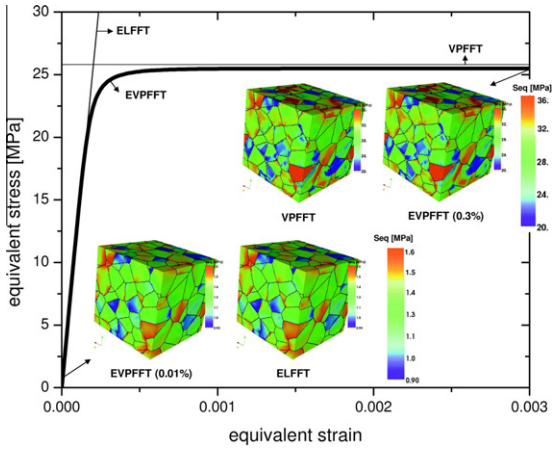

Fig. 1. Equivalent stress–strain curve predicted with the EVP–FFT model using a 128 × 128 × 128 Fourier grid, for the case of a copper polycrystal with 100 grains, random texture and no strain-hardening, deformed in unixial tension up to 0.3%, and effective responses (initial elastic slope and saturated stress lines) predicted with EL-FFT for the same elastic constants, and VP-FFT for the same viscoplastic constitutive parameters. Also shown: equivalent stress fields predicted with EL-FFT and EVP–FFT at 0.01%, and with VP-FFT and EVP–FFT at 0.3%.

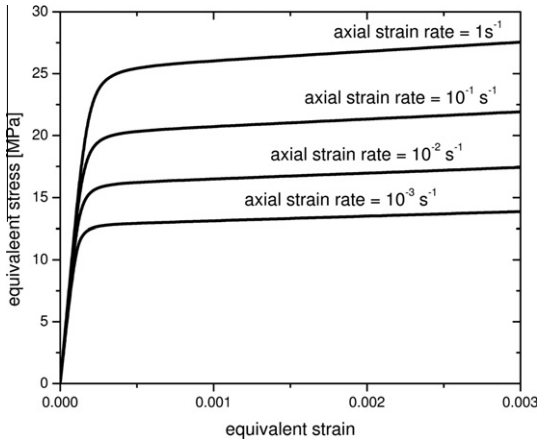

Fig. 2. Stress–strain curves predicted for the copper polycrystal, with linear hardening (H = 100 MPa), for four different values of the prescribed axial strain rate: $\dot{E}_{33} = 10^{-3}, 10^{-2}, 10^{-1}$ and 1 s^{-1}.

as the ones previously considered, but, in this case, in order to assess the rate-sensitivity of the model, four different values of the axial strain rate component were prescribed: $\dot{E}_{33} = 10^{-3}, 10^{-2}, 10^{-1}$ and 1 s^{-1}. The predicted final slope of the stress–strain curves and the relatively high strain-rate dependence of the effective response, corresponding to the relatively low stress exponent adopted, are well captured by the model.

Next, we present a convergence analysis of the proposed numerical method. Fig. 3 shows the convergence of two simulations for the copper polycrystal, deformed in uniaxial tension at a axial strain rate $\dot{E}_{33} = 1s^{-1}$, assuming no hardening (H = 0) and a very strong linear hardening (H = 1000 MPa, i.e. $H = 100 \times \tau_o^s$). Fig. 3(a) shows the effective stress–strain curves obtained after 15 steps of 0.01%. In order to compare the convergence rate in both cases, Fig. 3(b) and (c) show the average number (calculated over the entire Fourier grid) of N-R iterations required to solve Eq. (16), as a function of the accumulated number of (“global”) iterations of the EVP–FFT model, for the “no-hardening” and “hardening” cases, respectively. (Note that in Section 2.3 the N-R and global iterations are indicated by the supra-indices (j) and (i), respectively). The alternating white and gray regions represent the intervals of global iterations required to converge within each deformation increment. Fig. 3(d) and (e) show the average (calculated over the entire Fourier grid) of the difference between the stress fields $\sigma(\boldsymbol{x})$ and $\lambda(\mathbf{x})$, normalized by the effective equivalent stress, as a function of the total number of global iterations, in the no-hardening and hardening cases, respectively. From Fig. 3(b) and (c) it can be observed that for both cases the average number of N-R iterations decreases, as convergence is approached within each deformation step. However, in the non-hardening case, this average number of N-R iterations starts from smaller values at the beginning of each deformation step and reaches faster the value of 2 for every voxel. This difference reflects the approximation incurred in the hardening case by using the N–R Jacobian given by Eq. (20). In any case, the fact that after some number of global iterations within each deformation step

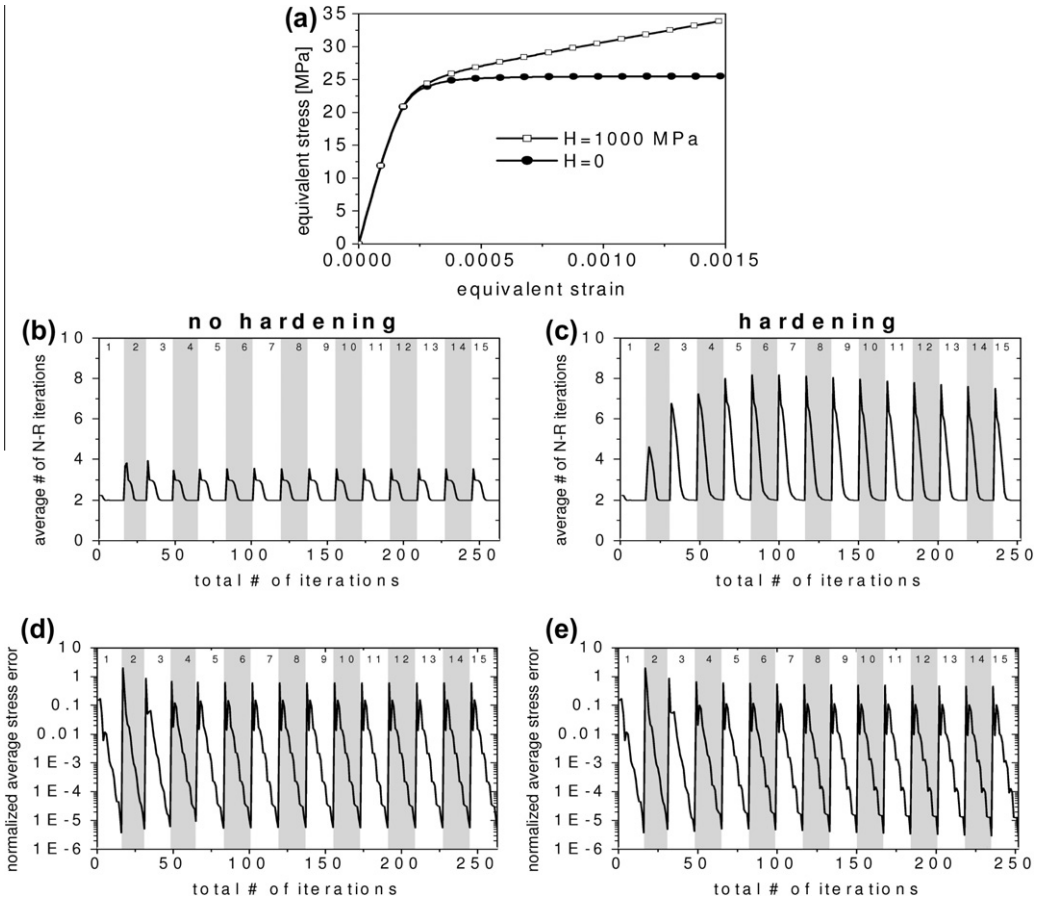

Fig. 3. Convergence of two simulations for the copper polycrystal, assuming no hardening ($H = 0$) and a very strong linear hardening ($H = 1000$ MPa). (a) Effective stress–strain curves up to 15 steps of 0.01%. (b) and (c) Average number of N-R iterations as a function of the accumulated number of global iterations of the EVP–FFT model, in the no hardening (b) and hardening (c) cases. (d) and (e) Normalized average difference between the stress fields $\boldsymbol{\sigma}(\mathbf{x})$ and $\boldsymbol{\lambda}(\mathbf{x})$, as a function of the total number of global iterations, in the no hardening (d) and hardening (e) cases.

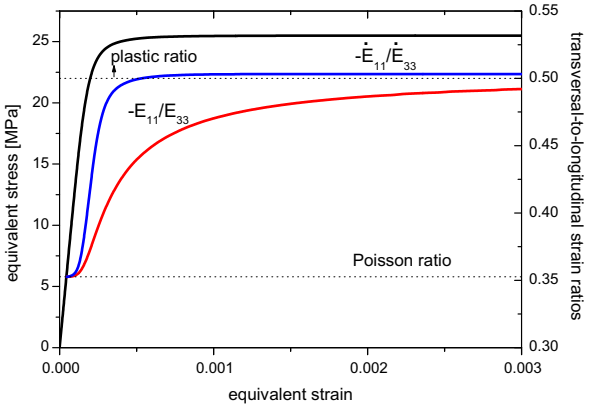

Fig. 4. Stress–strain curve for the copper polycrystal, in the case of uniaxial tension along x_3 ($\dot{E}_{33} = 1s^{-1}$ and $\Sigma_{11} = \Sigma_{22} = 0$ prescribed, Σ_{33}, $\dot{E}_{11}$ and $\dot{E}_{22}$ resulting from the predicted response), and evolution of the predicted transversal-to-longitudinal strain-rate ratio ($-\dot{E}_{11}/\dot{E}_{33}$), and total strain ratio ($-E_{11}/E_{33}$). The elastic (Poisson) and plastic transversal-to-longitudinal ratios also indicated.

every voxel requires only 2 N–R iterations reflects the goodness of the proposed Jacobian. On the other hand, Fig. 3(d) and (e) show that hardening has a very little effect on the number of global iterations required for convergence of the proposed FFT-based method.

The last benchmark consists in verifying the correct treatment of mixed boundary conditions. Fig. 4 displays the same stress–strain curve as shown in the first example for the case of uniaxial tension along x_3 of a non-hardening copper polycrystal (i.e. with $\dot{E}_{33} = 1s^{-1}$ and $\Sigma_{11} = \Sigma_{22} = 0$ prescribed, and, thus, Σ_{33}, $\dot{E}_{11}$ and $\dot{E}_{22}$ resulting from the predicted response). The other two curves show the predicted ("instantaneous") transversal-to-longitudinal strain rate ratio ($-\dot{E}_{11}/\dot{E}_{33}$), and the ("accumulated") ratio between the total strain components ($-E_{11}/E_{33}$). The instantaneous ratio starts at the value of 0.35, corresponding to the effective Poisson ratio of a random copper polycrystal, while, as the simulation goes through the elastoplastic transition into the fully-plastic regime, the latter rapidly increases, reaching a value of 0.5, corresponding to the transversal-to-longitudinal ratio associated with an incompressible axisymmetric plastic flow.

4. Application

After assessing our model with the above relatively simple but indispensable benchmarks, in this Section we show a first application of the EVP–FFT formulation to study the interplay between elastic and plastic anisotropy, and its effect on the effective behavior and local micromechanical response during the elastoplastic transition. Similar analysis of the role of texture and microstructure on the distribution of stress "hot spots" (i.e. local values of stress significantly above the average) was recently carried out by Rollett et al. (2010) using the VP version of the FFT formulation. Consequently, the conclusions of this earlier study were strictly only applicable to materials already deforming in a fully-plastic regime. The ability of carrying out similar hot-spot analysis using the EVP–FFT model allows us gaining new insights into the important regime of incipient plasticity, in which it is evident that extreme values statistics of the micromechanical fields very often play a dramatic role in determining macroscopic response, although the correlation between microstructure and those extreme values is not well understood.

To illustrate the feasibility of performing this kind of analysis using our new EVP–FFT tool, we compare simulations carried out for the same copper polycrystal studied in the previous Section (with $H = 100$ MPa), against the case of another "arti-

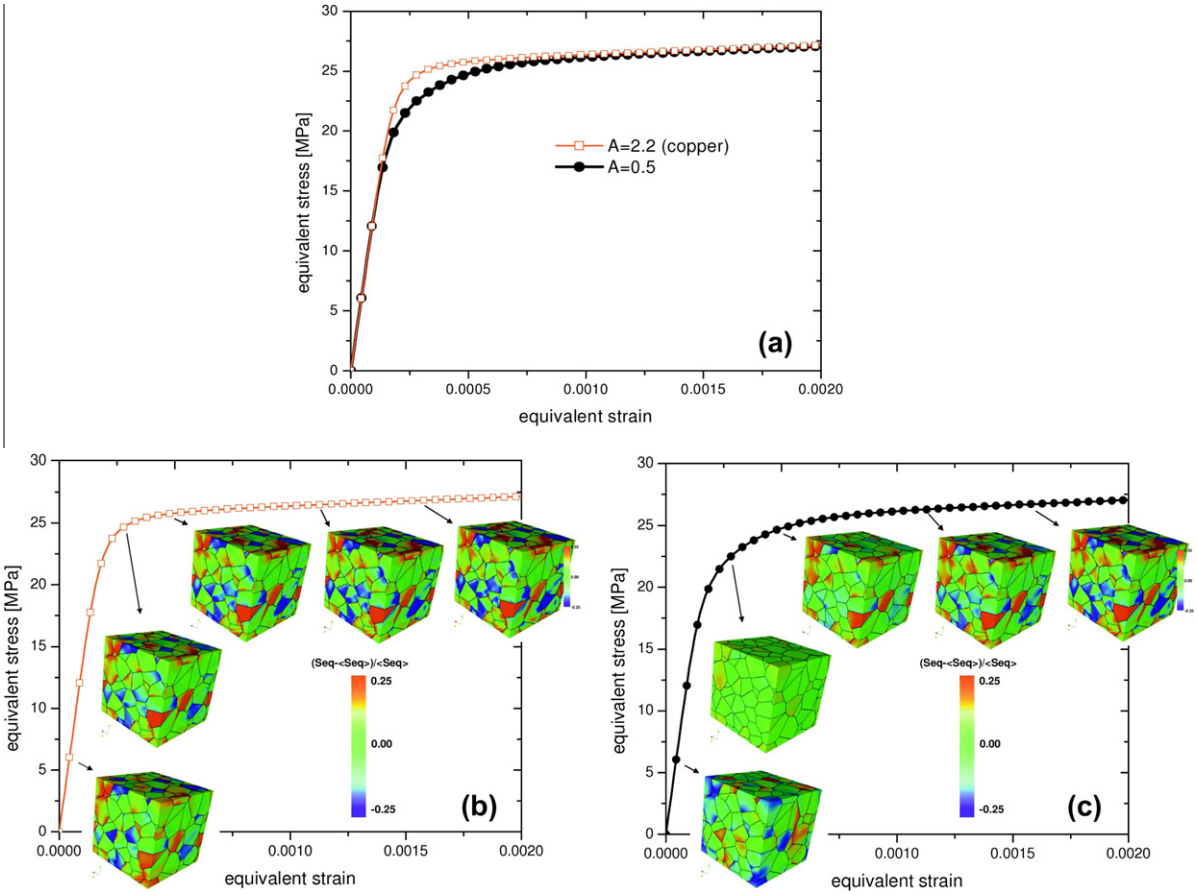

Fig. 5. (a) Effective response predicted with the EVP–FFT model for the copper polycrystal ($A = 2.2$) and the artificial fcc random polycrystal ($A = 0.5$) deformed in uniaxial tension up to 0.2%. (b) and (c) Predicted fields of normalized fluctuations of the von Mises stress, for the copper polycrystal (b) and the artifical fcc polycrystal (c), in different stages of the loading.

ficial" fcc polycrystal, having identical distribution of grains and orientations and same viscoplastic constitutive parameters, but different single crystal elastic anisotropy. At this point, it should be reminded that the elastic anisotropy parameter of a cubic single crystal is defined as $A = (2 \times C_{44})/(C_{11} - C_{12})$, which, in the case of the adopted elastic constants for copper, gives $A = 2.2$. Such value of $A > 1$ determines that, in a copper single crystal, e.g. $\langle 100 \rangle$ and $\langle 1\,1\,1 \rangle$ are soft and hard elastic directions, respectively. The same is true for the plastic anisotropy of a fcc single crystal deforming by $\{1\,1\,1\}\langle 1\,1\,0 \rangle$ slip. Meanwhile, for our artificial fcc single crystal, in order to reverse the elastic directional properties with respect to the plastic anisotropy while keeping the same effective elastic response, we have used a simple algorithm based on Hershey's (1954) elastic self-consistent formula for the effective response of a random cubic polycrystal with spherical grains. Prescribing $A = 0.5$, the values of C_{ij} that give the same effective elastic response (according to the elastic self-consistent model) as the copper polycrystal are: $C_{11} = 233.6$, $C_{12} = 88.2$ and $C_{44} = 33.8$ GPa.

Fig. 5(a) shows the effective stress–strain response for uniaxial tension along x_3 for an axial strain rate $\dot{E}_{33} = 1s^{-1}$ of the copper polycrystal ($A = 2.2$) and the artificial fcc polycrystal ($A = 0.5$), after 20 steps of 0.005%, up to a strain of 0.2%. The initial elastic and the stable fully-plastic responses are identical, but the stress–strain curves differ in the elastoplastic transition. In order to interpret this difference in effective behavior, Fig. 5(b) and (c) show the predicted fields of normalized fluctuations of the von Mises stress, for the copper and the artificial fcc polycrystal, respectively, in selected stages of the loading. Since, in the copper single crystal, the same crystallographic directions are relatively soft or hard, both elastically and plastically, the locations of the hot and cold spots of the stress field do not change throughout the deformation. On the other hand, since in the artificial single crystal the hard elastic crystal directions become soft plastic directions and vice versa, the elastic hot spots become plastic cold spots and vice versa, as the material goes through the elastoplastic transition. This switch results in an almost homogenous stress field approximately half-way through the transition. This hot spot/cold spot reversion very clearly observed at local level also has an effect on the effective response, giving a longer elastoplastic transition compared with the copper polycrystal, as seen in Fig. 5(a). This result shows that Rollett et al's. (2010) VP hot-spot analysis cannot automatically be extended to the incipient-plasticity regime, although the correlation between texture and microstructure and the location of VP hot spots may be also meaningful (at least qualitatively) in the incipient-plasticity regime in the cases of high SFE fcc materials (i.e. deforming exclusively by $\{1\,1\,1\}\langle 1\,1\,0 \rangle$ slip) with single crystal elastic anisotropy parameter $A > 1$ (e.g. Cu, Al, Fe).

5. Summary and perspectives

In this paper we have described the formulation, benchmarked our numerical implementation and presented a first application to stress hot-spot analysis, of the small-strain version of the EVP–FFT model for polycrystalline materials. The EVP–FFT formulation has also been extended to large strains and it is being reported elsewhere (Eisenlohr et al., in preparation). Depending on the specific need, the small-strain or large-strain versions of the model can be further utilized in a suite of applications requiring full-field polycrystal plasticity.

All the benchmarks and applications presented here correspond to a unit cell discretized using a $128 \times 128 \times 128$ grid, i.e. involving more than 2 million Fourier points. This resolution can be handled with 8 GB RAM and computing times of about 1 h per deformation increment. We have verified that going to the next level of refinement ($256 \times 256 \times 256$) produces very similar results, at the expense of 8 times more memory usage and at least 8 times more execution time. We have run the case reported in Fig. 5(a) with a 256^3 grid and compared the results with the 128^3 discretization of the same polycrystal. The predicted effective behavior is indistinguishable within the threshold error used in the iterative procedure. Meanwhile, the comparison between the mean value of the stress in the grains, averaged over the 100 grains, is better than 3×10^{-4}, relative to the effective stress, and the average normalized difference in local stresses, computed for every point in the coarser case against every other point in the more refined case is less than 2%.

Of particular interest are applications of the new EVP–FFT formulation for better interpretation of experimental data. For instance, the interpretation of neutron diffraction measurements of internal lattice (elastic) strains can benefit from the use of the EVP–FFT. Until now, the numerical approaches used to correlate texture and microstructure with lattice strains were based on self-consistent homogenization (e.g. Turner and Tomé, 1994; Clausen et al., 1998; Neil et al, 2010) or CP-FEM models (Dawson et al., 2001, 2005; Wong and Dawson, 2010). Homogenization-based models do a reasonably good job at matching some features of the distribution of internal strains measured with neutron diffraction, specially because the latter in general provides lattice strain measurements from a relatively large (statistically representative) polycrystalline volume containing a large number of grains. However, homogenization approaches cannot account for neighboring grain interactions and intragranular heterogeneity of the micromechanical fields. CP-FEM models, on the other hand, do account for grain-to-grain interactions and intragranular field variations, but the size of the volume element and the intra-grain resolution that can be investigated is limited, i.e. far from being statistically representative, with presently available computational resources. In contrast, the EVP–FFT formulation is able to deliver space-resolved predictions of elastic strains with high intragranular resolution, more efficiently than CP-FEM (Prakash and Lebensohn, 2009; Eisenlohr et al., in preparation). The first application of the EVP–FFT formulation to model neutron diffraction measurements of lattice strains evolution in fcc materials is being published elsewhere (Kanjarla et al., submitted for publication). Further on, we foresee 3-D space-resolved measurements of internal strains of individual grains in hcp (Aydiner et al., 2009) as well as in cubic aggregates (Oddershede et al., 2010, 2011) also being modeled with the EVP–FFT approach, with direct input and validation from such measurements.

Finally, we should mention another potential application of the proposed model. In the past the more restricted viscoplastic FFT-based formulation was applied to generate reference solutions, obtained by computing ensemble averages over multiple realizations of polycrystalline (Lebensohn et al., 2004a,b) and composites (Idiart et al., 2006) volume elements, for the assessment of different nonlinear homogenization models for viscoplastic heterogenous materials. On the other hand, several homogenization theories have being been recently proposed for the more general case of elasto-viscoplastic heterogeneous materials (Lahellec and Suquet, 2007a,b; Mercier and Molinari, 2009; Doghri et al., 2010). The proposed EVP–FFT can be useful to obtain reference solutions for comparison against estimates of these different theories, specialized to polycrystalline materials.

Acknowledgements

Ricardo A. Lebensohn wishes to thank Prof. Pierre Suquet (LMA, Marseille) for fruitful discussions. RAL also thanks the Humboldt Foundation for supporting his stay in Max-Planck-Institut für Eisenforschung (MPIE), Düsseldorf, through the Humboldt Research Award, as well as support from Joint DoD/DOE Munitions Technology Program and ASC Physics & Engineering Models, Materials Project. The work of Anand K. Kanjarla is supported by the US Department of Energy, Office of Basic Energy Sciences, project FWP-06SCPE401. The work of Philip Eisenlohr is supported by the Max-Planck Society as part of the Computational Mechanics of Polycrystals–CMCn initiative, a joint research group between MPIE and the Fraunhofer Institut für Werkstoffmechanik, Freiburg.

References

Asaro, R.J., Needleman, A., 1985. Texture development and strain hardening in rate dependent polycrystals. Acta Metallurgica 33, 923–953.
Aydiner, C.C., Bernier, J.V., Clausen, B., Lienert, U., Tome, C.N., Brown, D.W., 2009. Evolution of stress in individual grains and twins in a magnesium alloy aggregate. Physical Review B 80, 024113.
Barbe, F., Decker, L., Jeulin, D., Cailletaud, G., 2001a. Intergranular and intragranular behavior of polycrystalline aggregates. Part 1: FE model. International Journal of Plasticity 17, 513–536.
Barbe, F., Decker, L., Jeulin, D., Cailletaud, G., 2001b. Intergranular and intragranular behavior of polycrystalline aggregates. Part 2: Results. International Journal of Plasticity 17, 537–563.
Bhattacharyya, A., El-Danaf, E., Kalidindi, S.R., Doherty, R.D., 2001. Evolution of grain-scale microstructure during large strain simple compression of polycrystalline aluminum with quasi-columnar grains: OIM measurements and numerical simulations. International Journal of Plasticity 17, 861–883.
Brenner, R., Lebensohn, R.A., Castelnau, O., 2009. Elastic anisotropy and yield surface estimates of polycrystals. International Journal of Solids and Structures 46, 3018–3026.
Brisard, S., Dormieux, L., 2010. FFT-based methods for the mechanics of composites: a general variational framework. Computational Materials Science 49, 663–671.
Clausen, B., Lorentzen, T., Leffers, T., 1998. Self-consistent modelling of the plastic deformation of FCC polycrystals and its implications for diffraction measurements of internal stresses. Acta Materialia 46, 3087–3098.
Dawson, P., Boyce, D., MacEwen, S., Rogge, R., 2001. On the influence of crystal elastic moduli on computed lattice strains in AA-5182 following plastic straining. Materials Science and Engineering A 313, 123–144.
Dawson, P.R., Boyce, D.E., Rogge, R.B., 2005. Correlation of diffraction peak broadening to crystal strengthening in finite element simulations. Materials Science and Engineering A 399, 13–25.
Delannay, L., Jacques, P.J., Kalidindi, S.R., 2006. Finite element modeling of crystal plasticity with grains shaped as truncated octahedrons. International Journal of Plasticity 22, 1879–1898.
Diard, O., Leclercq, S., Rousselier, G., Cailletaud, G., 2005. Evaluation of finite element based analysis of 3D multicrystalline aggregates plasticity – Application to crystal plasticity model identification and the study of stress and strain fields near grain boundaries. International Journal of Plasticity 21, 691–722.
Doghri, I., Adam, L., Bilger, N., 2010. Mean-field homogenization of elasto-viscoplastic composites based on a general incrementally affine linearization method. International Journal of Plasticity 26, 219–238.
Eisenlohr, P., Diehl, M., Lebensohn, R.A., Roters, F., in preparation. Solving finite-deformation crystal elasto-viscoplasticity with a fast Fourier transform-based spectral method.
Eyre, D.J., Milton, G.W., 1999. A fast numerical scheme for computing the response of composites using grid refinement. Journal de Physique III 6, 41–47.
Hershey, A.V., 1954. The elasticity of an isotropic aggregate of anisotropic cubic crystals. Journal of Applied Mechanics – Transactions of the ASME 21, 236–240.
Idiart, M.I., Moulinec, H., Ponte Castañeda, P., Suquet, P., 2006. Macroscopic behavior and field fluctuations in viscoplastic composites: second-order estimates versus full-field simulations. Journal of the Mechanics and Physics of Solids 54, 1029–1063.
Kanjarla, A.K., Lebensohn, R.A., Balogh, L., Tomé, C.N., submitted for publication. Study of internal lattice strain distribution in stainless steel using full field elasto-viscoplastic formulation based on fast Fourier transforms. Acta Materialia.
Lahellec, N., Suquet, P., 2007a. On the effective behavior of nonlinear inelastic composites. I. Incremental variational principles. Journal of the Mechanics and Physics of Solids 55, 1932–1965.
Lahellec, N., Suquet, P., 2007b. On the effective behavior of nonlinear inelastic composites. II. A second-order procedure. Journal of the Mechanics and Physics of Solids 55, 1964–1992.
Lauridsen, E.M., Dey, S.R., Fonda, R.W., Juul-Jensen, D., 2006. Nondestructive approaches for 3-D materials characterization. Journal of the Minerals, Metals and Materials Society 58, 40–44.
Lebensohn, R.A., 2001. N-site modelling of a 3-D viscoplastic polycrystal using Fast Fourier Transform. Acta Materialia 49, 2723–2737.
Lebensohn, R.A., Liu, Y., Ponte Castañeda, P., 2004a. On the accuracy of the self-consistent approximation for polycrystals: comparison with full-field numerical simulations. Acta Materialia 52, 5347–5361.
Lebensohn, R.A., Liu, Y., Ponte Castañeda, P., 2004b. Macroscopic properties and field fluctuations in model power-law polycrystals: full-field solutions versus self-consistent estimates. Proceedings of the Royal Society of London A 460, 1381–1405.
Lebensohn, R.A., Brenner, R., Castelnau, O., Rollett, A.D., 2008. Orientation image-based micromechanical modelling of subgrain texture evolution in polycrystalline copper. Acta Materialia 56, 3914–3926.
Lebensohn, R.A., Montagnat, M., Mansuy, P., Duval, P., Meysonnier, J., Philip, A., 2009. Modeling viscoplastic behavior and heterogenous intracrystalline deformation of columnar ice polycrystals. Acta Materialia 57, 1405–1415.
Lee, S.B., Lebensohn, R.A., Rollett, A.D., 2011. Modeling the viscoplastic micromechanical response of two-phase materials using fast Fourier transforms. International Journal of Plasticity 27, 707–727.

Mercier, S., Molinari, A., 2009. Homogenization of elastic-viscoplastic heterogeneous materials: self-consistent and Mori–Tanaka schemes. International Journal of Plasticity 25, 1024–1048.
Michel, J.C., Moulinec, H., Suquet, P., 2000. A computational method based on augmented Lagrangians and fast Fourier transforms for composites with high contrast. Computer Modeling in Engineering and Sciences 1, 79–88.
Michel, J.C., Moulinec, H., Suquet, P., 2001. A computational scheme for linear and non-linear composites with arbitrary phase contrast. International Journal of Numerical Methods in Engineering 52, 139–158.
Mika, D.P., Dawson, P.R., 1998. Effects of grain interaction on deformation in polycrystals. Materials Science and Engineering A 257, 62–76.
Moulinec, H., Suquet, P., 1994. A fast numerical method for computing the linear and nonlinear mechanical properties of composites. C.R. Comptes Rendus de la Academie de Sciences Paris Serie II 318, 1417–1423.
Moulinec, H., Suquet, P., 1998. Numerical method for computing the overall response of nonlinear composites with complex microstructure. Computational Methods in Applied Mechanics and Engineering 157, 69–94.
Neil, C.J., Wollmershauser, J.A., Clausen, B., Tomé, C.N., Agnew, S.R., 2010. Modeling lattice strain evolution at finite strains and experimental verification for copper and stainless steel using in situ neutron diffraction. International Journal of Plasticity 26, 1772–1791.
Oddershede, J., Schmidt, S., Poulsen, H.F., Sorensen, H.O., Wright, J., Reimers, W., 2010. Determining grain resolved stresses in polycrystalline materials using three-dimensional X-ray diffraction. Journal of Applied Crystallography 43, 539–549.
Oddershede, J., Schmidt, S., Poulsen, H.F., Margulies, L., Wright, J., Moscicki, M., Reimers, W., Winther, G., 2011. Grain-resolved elastic strains in deformed copper measured by three-dimensional X-ray diffraction. Materials Characterization 62, 651–660.
Prakash, A., Lebensohn, R.A., 2009. Simulation of micromechanical behavior of polycrystals: finite elements vs. fast Fourier transforms. Modelling and Simulation in Materials Science and Engineering 17, 064010.
Raabe, D., Sachtleber, M., Zhao, Z., Roters, F., Zaefferer, S., 2001. Micromechanical and macromechanical effects in grain scale polycrystal plasticity experimentation and simulation. Acta Materialia 49, 3433–3441.
Rollett, A.D., Lebensohn, R.A., Groeber, M., Choi, Y., Li, J., Rohrer, G.S., 2010. Stress hot spots in viscoplastic deformation of polycrystals. Modelling and Simulation in Materials Science and Engineering 18, 074005.
Roters, F., Eisenlohr, P., Hantcherli, L., Tjahjanto, D.D., Bieler, T.R., Raabe, D., 2010. Overview of constitutive laws, kinematics, homogenization and multiscale methods in crystal plasticity finite-element modeling: theory, experiments, applications. Acta Materialia 58, 1152–1211.
Simmons, G., Wang, H., 1971. Single Crystal Elastic Constants and Calculated Aggregate Properties: A Handbook. MIT Press.
Turner, P.A., Tomé, C.N., 1994. A study of residual-stresses in zircaloy-2 with rod texture. Acta Metallurgica et Materialia 42, 4143–4153.
Uchic, M.D., Groeber, M.A., Dimiduk, D.M., Simmons, J.P., 2006. 3-D Microstructural characterization of nickel superalloys via serial-sectioning using a dual beam FIB-SEM. Scripta Materialia 55, 23–28.
Wong, S.L., Dawson, P.R., 2010. Influence of directional strength-to-stiffness on the elastic–plastic transition of fcc polycrystals under uniaxial tensile loading. Acta Materialia 58, 1658–1678.
Zeman, J., Vondrejc, I., Novak, J., Marek, I., 2010. Accelerating a FFT-based solver for numerical homogenization of periodic media by conjugate gradients. Journal of Computational Physics 229, 8065–8071.